Recombination of low energy electrons with U^{28+}

G. F. Gribakin and S. Sahoo

Department of Applied Mathematics and Theoretical Physics, Queens University, Belfast BT7 1NN, NI UK

V. Dzuba

School of Physics, University of New South Wales, Sydny 2052, Australia

Abstract. We performed an extensive study of configuration mixing between the doubly excited (doorway) states and complex multiply excited states of U^{28+} near its ionization threshold. The detailed investigation of complex spectrum and analysis of the statistics of eigenstate components show that the dielectronic (doorway) states weakly mixed with each other. However, they show substantial mixing with the complex multiply excited states. This situation explains the mechanism of low energy electron recombination with U^{28+} . We calculated the energy averaged capture cross sections as a sum over dielectronic doorway states and found our present calculation interprets well the experimental recombination rates in the energy range of 1 to 100 eV.

PACS numbers: PACS: 34.80.Lx, 31.10.+z, 34.10.+x, 32.80.Dz

1. Introduction

Atomic processes are of great importance from astrophysical and other various point of view. Especially the low energy recombination cross sections and rate coefficients are required for understanding the fusion and astrophysical plasmas. In particular dielectronic recombination (DR) plays a significant role in astrophysics because it is the dominant electron-ion recombination process for most ions in low density, photo-ionized and electron-ionized cosmic plasmas [1]. Accurate rate coefficients are needed to calculate reliably the ionization balance, thermal structure and line emission of cosmic plasmas. Most importantly the low energy positron antiproton recombination provides a challenging scheme for the production of antihydrogen[2].

It is well-known that due to the presence of additional recombination channels such as DR, the rate coefficients are found to be larger than radiative recombination (RR) rates for many electron complex ions. In DR process the incident electron is captured in a doubly-excited state of the compound ion, which is then stabilized by photoemission. This process originally suggested by J. Sayers and was first considered

by Massey and Bates [3] in the study of ionospheric oxygen. Electron-ion recombination has been measured directly in the laboratory since early 1980's [4]. More recently the use of heavy-ion accelerators and electron coolers of ion storage rings has greatly advanced the experiment [5, 6]. Recombination rates for various ions have been measured at electron energies from threshold to hundreds of electron volts (eV) with a fraction-ofan-eV resolution [7, 8, 9, 10, 11, 12, 13]. For few-electron ions the measured rates were found to be in good agreement with theoretical predictions which included the contribution of DR resonances on top of the RR background, e.g., in He⁺ [14], Li-like C⁴⁺ [13] and Ar¹⁵⁺ [7, 12], and B-like Ar¹³⁺ [15]. However, more complicated ions, e.g., Au⁵⁰⁺ [11], U²⁸⁺[10] and Au²⁵⁺[16], showed complicated resonance spectra and stronglyenhanced recombination rates at low electron energies. The Au²⁵⁺ ion has been studied in detail by Gribakin et al.[18] and Flambaum et al.[20] using statistical methods. They suggested that the strongly enhanced low energy electron recombination observed in this ion is mediated by complex multiply-excited states rather than simple dielectronic resonances and the dielectronic resonances play the role of doorways to the electron capture process. The statistical method developed by Flambaum et al. [20] is based on the assumption of strong (chaotic) configuration mixing. This assumption has been verified by Gribakin and Sahoo [19] in a recent study. However, for U²⁸⁺, no theory so far has described the low energy DR process successfully.

Historically the recombination rate enhancement was observed first in $U^{28+}[10]$. This measurement has been performed in a merged beam experiments at UNILAC accelerator in Darmstadt and at heavy-ion storage ring TSR in Heidelberg. experiment found rate enhancement in the U²⁸⁺ spectrum exceeds the theoretical calculation by at least a factor 20 in the energy range below 10 eV. Later in 1998, they extended the experiment to high energies up to 420 eV [17] and a comparison has been made with the theoretical calculations which is based on distorted wave approximations. The DR cross sections are calculated in this method are able to explain the main resonant features in the range 80–180 eV, but failed to identify the resonances and reproduce the rate at smaller energies. The cross sections involving the excitations from the 5s²5p² ground state configuration calculated in this method are well described by using either semirelativistic wave functions as found in AUTOSTRUCTURE codes or fully relativistic wave functions in HULLAC codes. However, the resonance structure observed at low energies i.e. below 80 eV largely remains unexplained. They finally concluded that in complex ions, particularly in U²⁸⁺ ion, what are the resonances just above the threshold and how they contribute to the low energy recombination remain a 'mystery'. In this paper we performed an extensive study of the excited spectra and eigenstates of U²⁸⁺ near its ionization threshold and calculated recombination rate coefficients for electron recombination with U^{28+} . We identified some of the resonances near the threshold those contribute significantly to the low energy recombination. The present results are found to be in good agreement with the experiment. This work develops further a statistical theory towards the full understanding of the mechanism of low energy electron recombination with U^{28+} and other similar complex ions.

2. Many-electron excitations

We consider the recombination of an electron with U^{28+} . Due to electron correlation the slow electron can be captured in one of the excited states of the compound ion U^{27+} . It has 65 electrons and its ground state configuration belongs to $1s^2$ $5s^25p^3$. Figure 1 shows the spectrum of relativistic nlj orbitals obtained by relativistic Hartree-Fock calculations. Atomic units (a.u.) are used unless otherwise stated. All the occupied orbitals below fermi level ($\sim 31.19~a.u.$) are obtained by a self consistent calculation of U^{28+} ground state. Each of excited orbitals above the fermi level are calculated by placing one electron on to it in the frozen $1s^2$ $5s^25p^2$ (U^{28+}) core. Our configuration interaction (CI) calculation shows that the ground state of U^{28+} and U^{27+} ions are characterized by their total angular momentum J=0.0 and 1.5 respectively. The difference between their total energies -27741.40 a.u. and -27771.37 a.u., gives us an estimation of ionization threshold (I.T.) = 29.97 a.u. (815.184 eV).

The excited states of the ion are generated by transferring one, two, three, etc., electrons from the ground state into the empty orbitals above fermi level. Since we are interested in the excited spectrum of the ion near its ionization threshold (29.97 a.u.), we consider it as a system of having only 29 electrons above the frozen Kr-like $1s^2....4p^6$ core. The number of many-electron states obtained by distributing 29 electrons over 40 relativistic orbitals, $4d_{3/2}$ through to $8g_{9/2}$ are huge in number. It is practically impossible to perform a CI calculation for all of them. We construct the excite spectrum by using mean field approach by calculating their mean energies E_i , and number of many electron states N_i associated with each of them:

$$E_i = E_{core} + \sum_a \epsilon_a n_a + \sum_{a < b} \frac{n_a (N_b - \delta_{ab})}{1 + \delta_{ab}} U_{ab}, \tag{1}$$

$$N_i = \prod_a \frac{g_a!}{n_a!(g_a - n_a)!},\tag{2}$$

where n_a are the orbital occupation numbers of the relativistic orbitals in a given configuration and $\sum_a n_a = n$. $\epsilon_a = \langle a|H_{core}|a \rangle$ is the s

ingle-particle energy of the orbital a in the field of the core, $g_a = 2j_a + 1$, and U_{ab} are the average Coulomb matrix elements for the electrons in orbitals a and b (direct minus exchange):

$$U_{ab} = \frac{g_a}{g_a - \delta_{ab}} \left[R_{abab}^{(0)} - \sum_{\lambda} \delta_p R_{abba}^{(\lambda)} \left\{ \begin{array}{cc} j_a & j_b & \lambda \\ \frac{1}{2} & -\frac{1}{2} & 0 \end{array} \right\}^2 \right]$$
(3)

 $R_{abba}^{(\lambda)}$ is the two-body radial Coulomb integral of λ multipole, and $\delta_p = 1$ when $l_a + l_b + \lambda$ is even and 0 otherwise. Using Eqs. (1)-(3) we obtained about 353 configurations within \pm 1 a.u. of ionization threshold. They comprise a total of 1.9×10^5 many electron states. The single-particle spectrum of U²⁸⁺ does not show large

gaps. Owing to the "gapless" single-particle spectrum, the density increases rapidly as a function of energy, as described by the Fermi-gas-model ansatz [21]

$$\rho(E) = AE^{-\nu} \exp(a\sqrt{E}),\tag{4}$$

with A=0.0885, $\nu=2.33$, and a=3.99 a.u.[23], where E is the energy above the ground state in atomic units. Figure 2 shows the level density calculated by averaging with a Gaussian with 1 a.u. variance. This figure depicts the level densities for both odd and even parity configurations. Also included in the figure are only the doubly excited configurations of even and odd parity found within \pm 1 a.u. of ionization threshold. It is found that the level density of the odd configurations near its ionization threshold is of the order is of 1×10^5 and

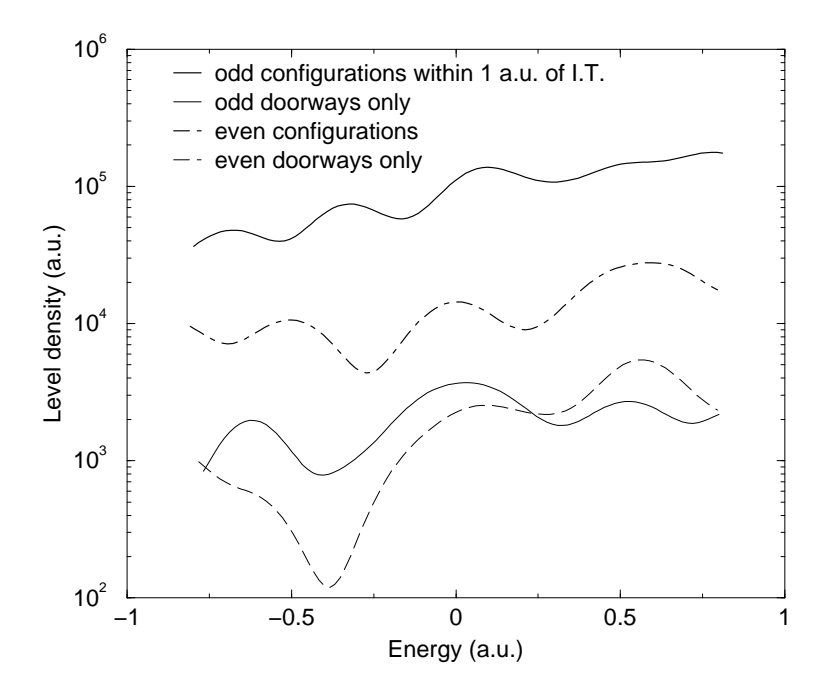


Figure 1. Level densities in U^{28+} within ± 1 a.u. of Ionization threshold. Thick solid line: odd configurations, Thin solid line: odd dielectronic configurations, Dash-dot line: even configurations and dashed line: even dieclectronic configurations.

those of even configurations it is of the order of 1.3×10^4 . This provides an evidence that this system is characterized by huge level density. This system may be compared with $\mathrm{Au^{25+}}$, in which the level density near its ionization threshold is about $1 \times 10^7 [18]$. This shows that $\mathrm{U^{28+}}$ ion is less complicated than $\mathrm{Au^{25+}}$ from the view point of dense excited spectrum. Apart from this one can estimate the mean level spacing from the distribution of total angular momentum J as shown in Figure 3.

Ionic eigenstates are characterized by their total angular momentum and parity J^{π} , and are 2J+1 times degenerate. Therefore the total level density can be broken into a sum of partial level densities: $\rho(E) = \sum_{J^{\pi}} (2J+1)\rho_{J^{\pi}}(E)$. The excitation spectrum of U²⁸⁺ near the ionization threshold, $E = I \approx 29.97$ a.u., contains many J ranging

from $\frac{1}{2}$ to $\frac{25}{2}$. Their distribution is in agreement with statistical theory [21, 22], which predicts that at a given energy $\rho_{J^{\pi}}$ are proportional to the function

$$f(J) = \frac{2(2J+1)}{(2J_m+1)^2} \exp\left[-\frac{(2J+1)^2}{2(2J_m+1)^2}\right],\tag{5}$$

where J_m is the most abundant J value. Numerically for U^{27+} we find $J_m \approx \frac{7}{2}$.

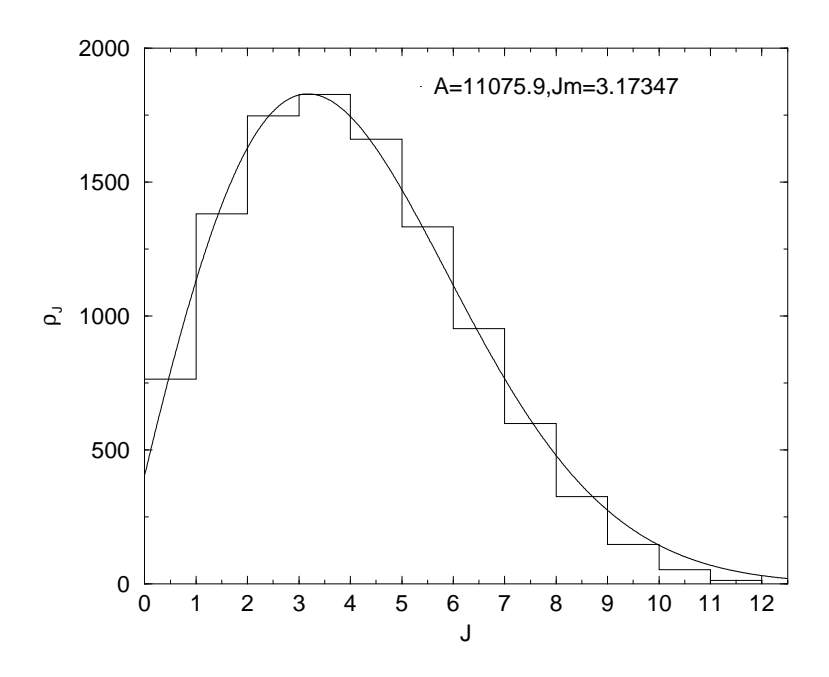


Figure 2. Densities of states with different J near ionization threshold of U^{28+} . Histograms show their distribution and the solid line is non linear fitting obtained from Eq.(5) which predicts the most abundant value of $J \sim 3.2$ and the proportionality constant \pm 11075.9.

Using Eq. (5) one can estimate the partial densities by $\rho_J = \rho_{J^+} + \rho_{J^-} \simeq f(J)\rho/\langle 2J+1\rangle$, where $\langle 2J+1\rangle$ is an average over f(J). For the most abundant angular momenta $J \sim J_m$, and assuming $\rho_{J^+} \approx \rho_{J^-}$, we have $\rho_{J^\pi}(E) = A_{J^\pi}E^{-\nu}\exp(a\sqrt{E})$. Near the ionization threshold this gives $\rho_{J^\pi} \approx 1.8 \times 10^3$ a.u. (Fig. 3), which means that the spacing between the multiply-excited states with a given J^π is small: $D = 1/\rho_{J^\pi} \sim 15$ meV. Whereas in Au^{25+} it is about 1 meV, i.e. 15 times larger than that found in Au^{25+} . This situation explains why individual resonances appear in recombination rates of U^{28+} but the same is not observed in Au^{25+} experimentally even at an energy resolution of 0.1 eV. However, the large density of multiply-excited states is only a "kinematic" reason behind the experimental observation. To explain the fact that the electron can actually be captured into these states, we need to analyze the dynamics of electron capture and show that the residual Coulomb interaction between the electrons (i.e. that beyond the mean field) makes for an efficient capture and accounts for the observed enhanced recombination rate.

3. Configuration mixing

Taking into account the fact that the rasidual Coulomb interaction is the key problem in many-electron processes, we construct the basis of many-electron states Φ_k from single-particle (e.g., Dirac-Fock) orbitals, and solve the eigenvalue problem for the Hamiltonian matrix $H_{ik} = \langle \Phi_i | \hat{H} | \Phi_k \rangle$, which yields the eigenvalues E_{ν} and eigenstates $|\Psi_{\nu}\rangle = \sum_{k} C_{k}^{(\nu)} |\Phi_{k}\rangle$ of the system (configuration interaction method). We performed two sets of model calculations. One include all the configurations within ± 1 a.u. of ionization threshold of U²⁸⁺, which produces 2516 states for $J^{\pi} = \frac{7}{2}^{-}$ sequence. Similarly the second calculation includes all the dielectronic (doorway) states within ± 1 a.u. of ionization threshold and produces 108 states for $J^{\pi} = \frac{7}{2}^{-}$ sequence. This shows that the number of states associated with the dielectronic configurations for a given J^{π} are not large in number. As a result we performed the full CI calculations for Hamiltonian matrix of size 108 and 2516 respectively and obtained the eigen values and eigenstate components. To study the mixing between the doubly excited states we analyze the eigenstate components by calculating the weight of a given doorway configuration shown in Figure 4(a)-(e). The weight (w) of a doorway state can be calculated as $\sum_{k=1,Nc} |C_k^{\nu}|^2$, where N_c is the number of states in each configuration. It has been shown in Ref[19] that when there is strong and uniform configuration mixing the weights significantly reduce from 1, but in the present case the weights go down from 1 but not significantly. So one can say that these doubly excited (doorways) states weakly mix with each other. When they are included in the large calculation (2516 states), their weights significantly go down from 1 as shown in Figure 4(f)-(j). This gives a signature of strong mixing i.e., the doorways show a significant mixing with multiply excited states. It has also been observed that the multiply excited configurations mix with each other quite comfortably. This mixing is mainly responsible for an enhancement of recombination rates over RR. In the recombination cross sections, the doorways which do not mix completely with either multiply excited states or with other doorways (in a sense they remain 'isolated') appear in the form of narrow peaks (resonances) which explains the experiment as well as the theory [17].

On the other hand, when the level density is high and the two-body interaction is sufficiently strong the system is driven into a regime of many-body quantum chaos, where the effect of configuration mixing can be described statistically in the case of $\operatorname{Au}^{25+}[18]$. This regime is characterized by the following [26, 27]. (i) Each eigenstate contains a large number N of principal components $C_k^{(\nu)} \sim 1/\sqrt{N}$, corresponding to the basis states Φ_k which are strongly mixed together. (ii) Owing to the strong mixing, the only good quantum numbers that can be used to classify the eigenstates, are the exactly conserved total angular momentum and parity J^{π} and the energy. (iii) The degree of mixing in this regime is in some sense complete, i.e. all basis states that can be mixed (within a certain energy rage, see below) are mixed. The notion of configurations based on the single-particle orbitals becomes largely irrelevant for the purpose of classifying the eigenstates. Each eigenstate contains substantial contributions of a few nearby

configurations. As mentioned above, in the present case we found that there is a weak configuration mixing between the dielectronic doorway configurations and complicated multiply excited states, and the multiply excited states show a substantially strong configuration mixing with each other. But the degree of mixing is not sufficiently strong to drive the system into chaotic regime.

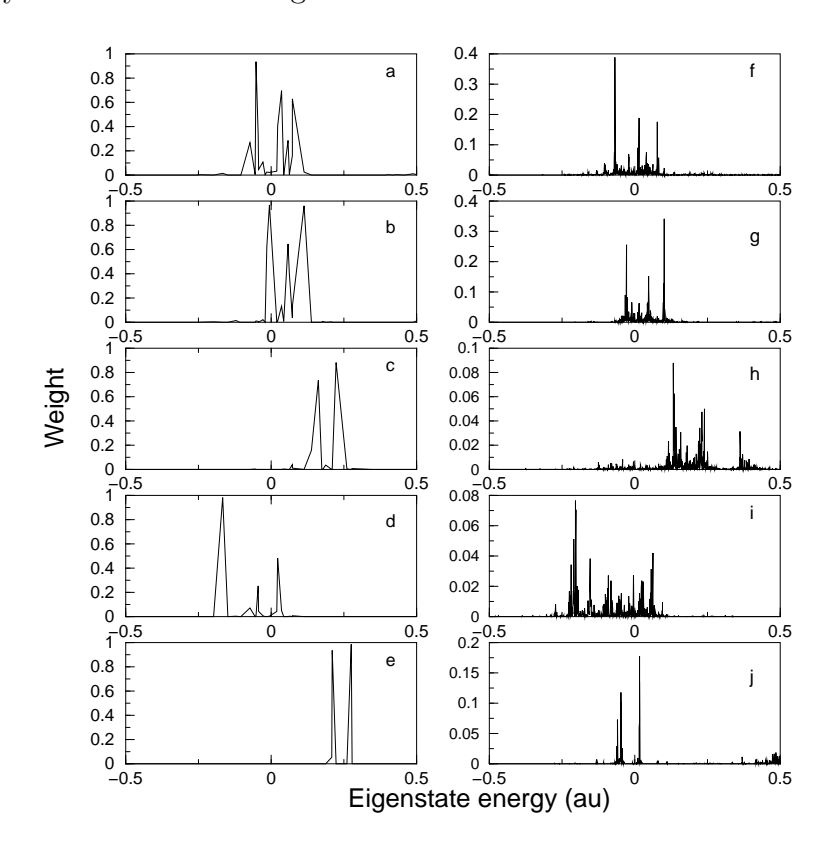


Figure 3. Weights of odd dielectronic doorway states obtained from two different calculations. Figure (a)-(e) are the weights of doorways obtained from a calculation involving 108 states. Figure (f)-(j) are the weights of the same doorways obtained from a calculation involving 2516 states

$$\begin{array}{l} \text{(a):} 4d_{3/2}^4 4d_{5/2}^6 4f_{5/2}^6 4f_{7/2}^7 5s_{1/2}^2 5p_{1/2}^2 5p_{3/2}^1 7f_{5/2}^1 (N_c \! = \! 4) \\ \text{(b):} 4d_{3/2}^4 4d_{5/2}^6 4f_{5/2}^6 4f_{7/2}^7 5s_{1/2}^2 5p_{1/2}^2 5p_{3/2}^1 7f_{7/2}^1 (N_c \! = \! 4) \\ \text{(c):} 4d_{3/2}^4 4d_{5/2}^6 4f_{5/2}^6 4f_{7/2}^8 5s_{1/2}^2 5p_{1/2}^1 5g_{9/2}^1 6p_{3/2}^1 (N_c \! = \! 2) \\ \text{(d):} 4d_{3/2}^4 4d_{5/2}^6 4f_{5/2}^6 4f_{7/2}^8 5s_{1/2}^1 5p_{1/2}^2 5d_{5/2}^1 7f_{5/2}^1 (N_c \! = \! 2) \\ \text{(e):} 4d_{3/2}^4 4d_{5/2}^6 4f_{5/2}^8 4f_{7/2}^8 5s_{1/2}^2 5p_{1/2}^2 5f_{5/2}^1 6p_{1/2}^1 (N_c \! = \! 2) \end{array}$$

 N_c is the number of states associated with each of the configurations.

This feature can be studied from the inverse participation ratio (IPR): $\Sigma_{j=1,Nc}|C_k^{\nu}|^{-4}$. Figure 5 shows the inverse participation ratio for the two sets of model calculations. The top figure depicts the inverse participation ratio of the doorways only and the middle one for the large (2516 states) calculation that includes all the configurations (both dielectronic and multiply excited states). We found most of the doorways are associated with number of states either 4 or 2 or even less. The top figure

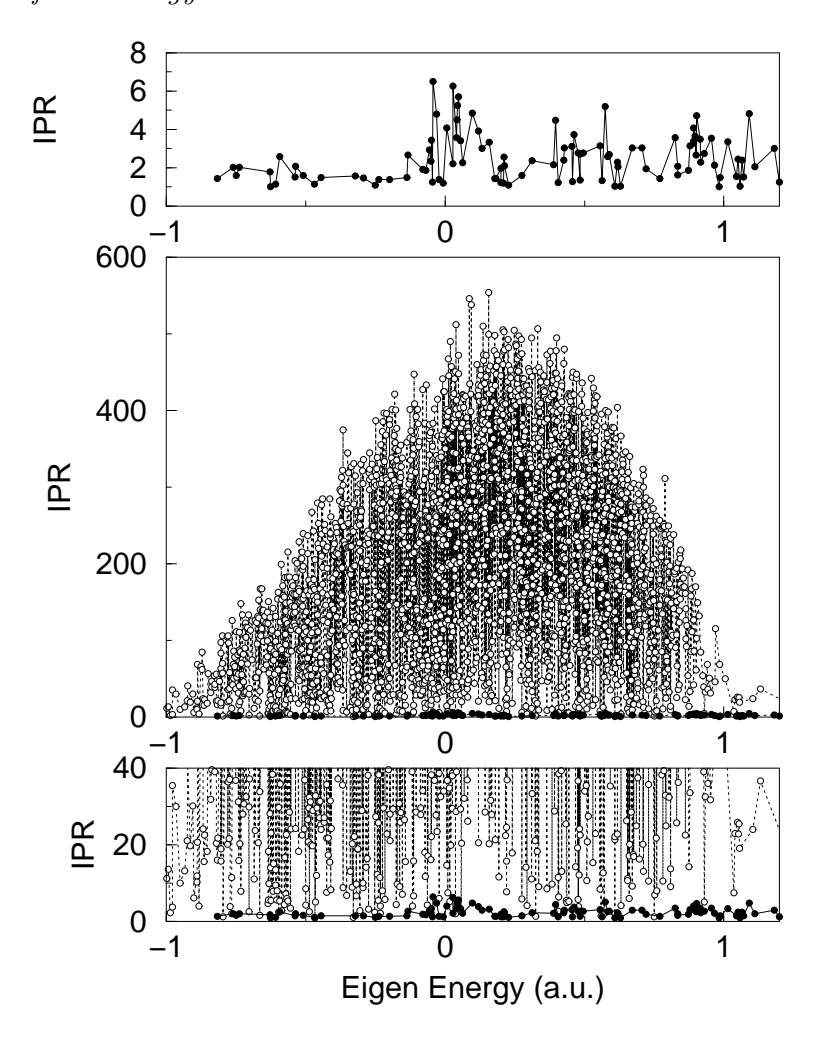


Figure 4. Inverse participation ratio (IPR). Top figure: for doorways having 108 states, the middle figure: for all configurations having 2516 states and the bottom one is same as middle figure but in an extended scale.

shows that the inverse participation ratio lies flat between 2 and 4 except at the energy range where the eigen energies are close to the ionization threshold. This indicates that a few number of the doorways having energies close to the threshold participate in mixing. However the middle figure shows a picture of strong but non uniform mixing which involves a lots of multiply excited states. When we included the IPR of doorways with the IPR obtained from large calculation as shown in the bottom figure, it lies well below as indicated by solid circles. It also provides us with an information that some of the doorways take part in mixing with multiply excited configurations and other doorways are weakly mixed or even remain isolated.

This strong mixing takes place in a certain energy range $|E_k - E_{\nu}| \lesssim \Gamma_{\rm spr}$, where $E_k \equiv H_{kk}$ is the mean energy of the basis state and $\Gamma_{\rm spr}$ is the so-called *spreading width*. More precisely, the mean-squared value of $C_k^{(\nu)}$ as a function of $E_k - E_{\nu}$, can be described

by a Breit-Wigner (BW) formula

$$\overline{\left|C_k^{(\nu)}\right|^2} = N^{-1} \frac{\Gamma_{\text{spr}}^2/4}{(E_k - E_\nu)^2 + \Gamma_{\text{spr}}^2/4},$$
 (6)

with $N = \pi \Gamma_{\rm spr}/2D$ fixed by normalization $\sum_k \left| C_k^{(\nu)} \right|^2 \simeq \int \overline{\left| C_k^{(\nu)} \right|^2} dE_k/D = 1$.

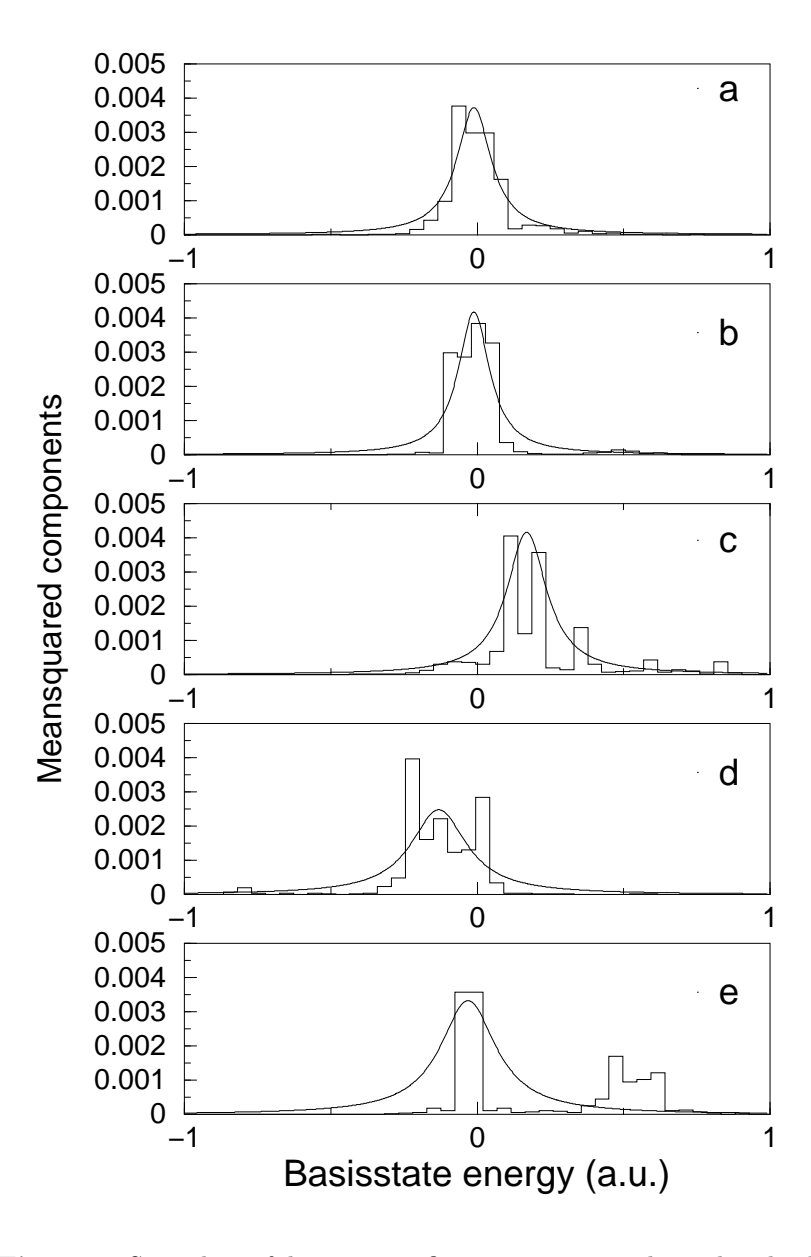


Figure 5. Spreading of doorway configurations in complicated multiply excited states obtained from 2516 x 2516 calculations for $J^{\pi}=3.5^-$ sequence. Each of the doorway configuration spreads as (a) 0.1433 a.u., (b) 0.1310 a.u., (c) 0.1661 a.u., (d) 0.2321 a.u. and (e) 0.2310 a.u.. These doorways are same as indicated in Fig4.

The mean-squared components are obtained by averaging over the basis states associated with each of the doorway configurations and are plotted as a function of eigen energies. We obtained $\Gamma_{\rm spr}$ of doorways (close to the ionization threshold) from

the BW fit which is shown in Figure 6(a)-(e). From the BW fit we observed that the $\Gamma_{\rm spr}$ is not constant and it varies from 0.1 a.u. to 0.2 a.u. in these doorways. There may be doorways which even show much less spreading. Roughly one can say the mixing takes place within 0.1 a.u.. So we calculated the recombination rates with two different values of spreading width which can be found in section IV. It may be pointed out that though the single BW fit is not as accurate as it should be, still it gives an estimation of the important quantity i.e. $\Gamma_{\rm spr}$. It is worth mentioning that the spreading width found in ${\rm Au^{25+}}$ is about 0.5 a.u.[18] and these value does not change if one performs calculations by adding more configurations[19].

4. Recombination

4.1. Theory

For low-energy electrons the contribution of the autoionising states (resonances) to the recombination cross section is given by (see, e.g., Ref. [24])

$$\sigma_r = \frac{\pi}{k^2} \sum_{\nu} \frac{2J+1}{2(2J_i+1)} \frac{\Gamma_{\nu}^{(r)} \Gamma_{\nu}^{(a)}}{(\varepsilon - \varepsilon_{\nu})^2 + \Gamma_{\nu}^2 / 4},\tag{7}$$

where $\varepsilon = k^2/2$ is the electron energy, J_i is the angular momentum of the initial (ground) target state, J are the angular momenta of the resonances, $\varepsilon_{\nu} = E_{\nu} - I$ is the position of the ν th resonance relative to the ionization threshold of the compound (final-state) ion, and $\Gamma_{\nu}^{(a)}$, $\Gamma_{\nu}^{(r)}$, and $\Gamma_{\nu} = \Gamma_{\nu}^{(r)} + \Gamma_{\nu}^{(a)}$ are its autoionisation, radiative, and total widths, respectively [25]. When the resonance spectrum is dense, σ_r can be averaged over an energy interval $\Delta \varepsilon$ which contains many resonances, $D \ll \Delta \varepsilon \ll \varepsilon$, yielding

$$\bar{\sigma}_r = \frac{2\pi^2}{k^2} \sum_{J^{\pi}} \frac{2J+1}{2(2J_i+1)D} \left\langle \frac{\Gamma_{\nu}^{(r)} \Gamma_{\nu}^{(a)}}{\Gamma_{\nu}^{(r)} + \Gamma_{\nu}^{(a)}} \right\rangle, \tag{8}$$

where $\langle ... \rangle$ means averaging. If the fluorescence yield, $\omega_f \equiv \Gamma_{\nu}^{(r)}/(\Gamma_{\nu}^{(r)} + \Gamma_{\nu}^{(a)})$, fluctuates weakly from resonance to resonance (see below), one can write $\bar{\sigma}_r = \bar{\sigma}_c \omega_f$, where

$$\bar{\sigma}_c = \frac{\pi^2}{k^2} \sum_{I^{\pi}} \frac{(2J+1)\Gamma^{(a)}}{(2J_i+1)D} \tag{9}$$

is the energy-averaged capture cross section, and $\Gamma^{(a)}$ is the average autoionisation width.

In a situation when there is a strong configuration mixing between the dielectronic doorway states and multiply excited states, the capture cross sections can be obtained as a sum over the single-electron excited states α , β and hole states γ , as well as the partial waves lj of the continuous-spectrum electron ε . As a result, we have

$$\begin{split} \bar{\sigma}_{c} &= \frac{\pi^{2}}{k^{2}} \sum_{\alpha\beta\gamma,lj} \frac{\Gamma_{\mathrm{spr}}}{(\varepsilon - \varepsilon_{\alpha} - \varepsilon_{\beta} + \varepsilon_{\gamma})^{2} + \Gamma_{\mathrm{spr}}^{2}/4} \sum_{\lambda} \frac{\langle \alpha,\beta \| V_{\lambda} \| \gamma, \varepsilon lj \rangle}{2\lambda + 1} \\ &\times \left[\langle \alpha,\beta \| V_{\lambda} \| \gamma, \varepsilon lj \rangle - (2\lambda + 1) \sum_{\lambda'} (-1)^{\lambda + \lambda' + 1} \left\{ \begin{matrix} \lambda & j_{\alpha} & j \\ \lambda' & j_{\beta} & j_{\gamma} \end{matrix} \right\} \langle \alpha,\beta \| V_{\lambda'} \| \varepsilon lj, \rangle \right] \end{split}$$

where ε_{α} , ε_{β} and ε_{γ} are the orbital energies, the two terms in square brackets represent the direct and exchange contributions, and $\langle \alpha, \beta || V_{\lambda} || \gamma, \varepsilon l j \rangle$ is the reduced Coulomb matrix element (see Ref.[20]).

It is assumed that the energies of dielectronic doorway states relative to the threshold is given by $\varepsilon_{\alpha} + \varepsilon_{\beta} - \varepsilon_{\gamma}$. A more accurate value can be obtained by using mean field energies (configuration energies) of doorway configurations in Eq.(10). The effect of using these two different energies can be found in next subsection. We have also shown the qualitative difference between the results obtained by using two different values of Γ_{spr} . Because Γ_{spr} is well defined in the case of a strong and chaotic configuration mixing. However, it can not be properly defined if the mixing of the configurations is weak and non-uniform.

Equation (10) is directly applicable to targets with closed-shell ground states. If the target ground state contains partially occupied orbitals, a factor

$$\frac{n_{\gamma}}{2j_{\gamma}+1}\left(1-\frac{n_{\alpha}}{2j_{\alpha}+1}\right)\left(1-\frac{n_{\beta}}{2j_{\beta}+1}\right),\tag{11}$$

where n_{α} , n_{β} , and n_{γ} are the orbital occupation numbers in the ground state Φ_i , must be introduced on the right-hand side of Eq. (10). Steps similar to those that lead to Eq. (10) were used to obtain mean-squared matrix elements of operators between chaotic many-body states [27, 28].

The chaotic nature of the multiply-excited states Ψ_{ν} can also be employed to estimate their radiative widths $\Gamma_{\nu}^{(r)}$. Electron-photon interaction is described by a single-particle dipole operator \hat{d} . Any excited electron in Ψ_{ν} may emit a photon, thus leading to radiative stabilization of this state. The total photo-emission rate $\Gamma_{\nu}^{(r)}$ can be estimated as a weighted sum of the single-particle rates,

$$\Gamma_{\nu}^{(r)} \simeq \sum_{\alpha,\beta} \frac{4\omega_{\beta\alpha}^3}{3c^3} |\langle \alpha \| \hat{d} \| \beta \rangle|^2 \left\langle \frac{n_{\beta}}{2j_{\beta} + 1} \left(1 - \frac{n_{\alpha}}{2j_{\alpha} + 1} \right) \right\rangle_{\nu}, \tag{12}$$

where $\omega_{\beta\alpha} = \varepsilon_{\beta} - \varepsilon_{\alpha} > 0$, $\langle \alpha || \hat{d} || \beta \rangle$ is the reduced dipole operator between the orbitals α and β , and $\langle \ldots \rangle_{\nu}$ is the mean occupation number factor. Since Ψ_{ν} have large numbers of principal components N, their radiative widths display small $1/\sqrt{N}$ fluctuations. This can also be seen if one recalls that a chaotic multiply-excited state is coupled by photoemission to many lower-lying states, and the total radiative width is the sum of a large number of (strongly fluctuating) partial widths. A similar effect is known in compound nucleus resonances in low-energy neutron scattering [21].

There is a certain similarity between Eqs. (10) and (12) and those for autoionisation and radiative rates obtained in a so-called configuration-average approximation [29]. In both cases the answers involve squares or products of two-body Coulomb matrix elements [see the direct and exchange terms in Eq. (10)], or single-particle dipole amplitudes [Eq. (12)]. However, there are a number of important differences between the present results and the configuration-average approximation. The latter considers dielectronic recombination and introduces averaging over configurations as a means of simplifying the calculation. The DR cross section is averaged over an arbitrary energy

interval $\Delta \varepsilon$, and only the configurations within this energy range contribute to the average. Effects of configuration mixing as well as level mixing within a configuration are neglected.

It is important to compare the radiative and autoionisation widths of chaotic multiply-excited states. Equation (12) shows that $\Gamma^{(r)}$ is comparable to the single-particle radiative widths. On the other hand, the autoionisation width $\Gamma^{(a)}$, is suppressed by a factor $\left|C_k^{(\nu)}\right|^2 \sim N^{-1}$ relative to that of a typical dielectronic resonance. Therefore, in systems with dense spectra of chaotic multiply-excited states the autoionisation widths are small. Physically this happens because the coupling strength of a two-electron doorway state to the continuum is shared between many complicated multiply-excited eigenstates. As a result, the radiative width may dominate the total width of the resonances, $\Gamma^{(r)} \gg \Gamma^{(a)}$, making their fluorescence yield close to unity. However, in the case of U^{28+} , $\Gamma^{(r)} \sim \Gamma^{(a)}$. Our numerical results for the recombination of U^{28+} presented in Sec. 4.2, confirm this scenario.

The resonance recombination cross section should be compared with the direct radiative recombination cross section

$$\sigma_d = \frac{32\pi}{3\sqrt{3}c^3} \frac{Z_i^2}{k^2} \ln\left(\frac{Z_i}{n_0 k}\right),\tag{13}$$

obtained from the Kramers formula by summing over the principal quantum number of the final state [18]. Here Z_i is the ionic charge ($Z_i = 28$ for U^{28+}), and n_0 is the principal quantum number of the lowest unoccupied ionic orbital ($n_0 = 5$). Note that the direct and energy-averaged resonance recombination cross sections of Eqs. (13) and (8) have similar energy dependences.

4.2. Numerical results

Numerical calculations of the cross section from Eqs. (10) and (11) involve summation over the orbitals shown in Fig. 1 with electron partial waves up to $i_{11/2}$. The results of the calculations for the recombination rates are displayed in Figure 7. We calculated the recombination rates using two different energies, i. e., configuration energies and relativistic energies. It is found that both the calculations are in good agreement. However, the magnitude of recombination rates obtained from both the present calculations lie above the experimental rates. This is due to the fact that we used $\omega_f = 1$ in the present calculations similar to that in Au²⁵⁺. It is clear that in the present case ω_f is less than 1 and remains constant throughout the energy range considered. The exchange contributions are found to be about 200 times smaller than the direct one so we did not include these when calculated the final rates. The radiative rates are found to be smaller in magnitude in comparison to DR rates and have almost negligible interference with the resonances. It may be pointed out that the present calculation with spreading width $\Gamma_{spr} \sim 0.15$ a.u, does not show enough resonance structures as have been observed in the experiment. Hence, we performed another calculation with $\Gamma_{spr} \sim 0.05$ a.u. and compared with the results obtained using spreading with 0.15 a.u. shown in

Figure 8. It is clear that the results do not show any change in magnitude. However, the calculation with $\Gamma_{spr} \sim 0.05$ interprets the resonance peaks very well which are in reasonable agreement with the experiment, though the position of peaks are different from the experiment. This is because the present energies of the doorway states are approximate and a few eV relative error is expected in this approach. The presence of narrow peaks in rate coefficients can be interpreted as: the dielectronic states which play the role doorway to the electron capture process weakly mix with each other as has been discussed in previous section and appear as single peaks. Because in statistical calculations one peak corresponds to one doorway state. It may be recalled that the distorted wave calculation[17], predicts the recombination rates in agreement with the experiment above 80 eV and below this energy the results are smaller in magnitude.

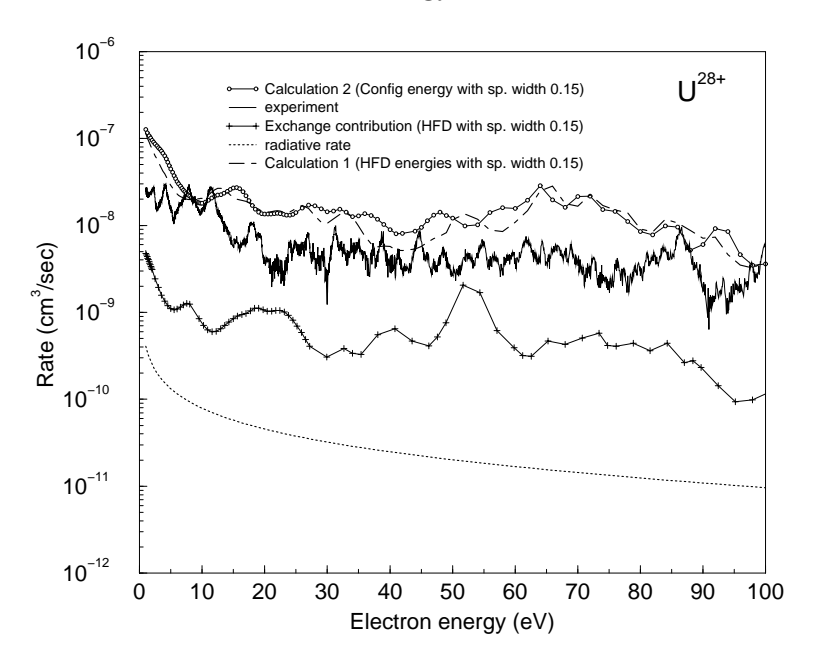


Figure 6. Electron recombination rate on U^{28+} . Open circles connected by solid line: Calculation 2 (using configuration energy and $\Gamma_{spread}=0.15$ a.u.), Dot-dashed line: Calculation 1 (using HFD energy and $\Gamma_{spread}=0.15$ a.u.), Solid lines: Experimental data, Solid line connected by plus sign: Exchange contribution (using HFD energy and $\Gamma_{spread}=0.15$ a.u.), Dotted line: Radiative rate.

Table 1 lists the most important dielectronic doorway contributions to the dimensionless sum in Eq. (10), which also determines the ratio of the autoionisation width to the spacing between the resonances. In total they account for about two thirds of the total cross section. Although these transitions have been selected according to the size of their contribution, their energies from two different calculations are close to the threshold, as seen in the last two columns in Table 1. Indeed, the spreading of configurations discussed in Sec. 2 allows configurations near the threshold, $|\Delta E| \lesssim \Gamma_{\rm spr}$, to contribute. On the other hand, the contribution of configurations lying far away from threshold, $|\Delta E| \gg \Gamma_{\rm spr}$, is suppressed. It may be pointed out that the theory of Mitnik et. al.[17] considers the excitations from 5s orbital only. However, the

Table 1. Electron orbitals which give the leading contribution to the low-energy (around 1 eV) electron recombination on U^{28+} .

Orbitals[1]				Direct	$\Delta E[3]$	$\Delta E[4]$			
α	β	γ	εlj	contribution[2]	(a.u.)	(a.u)			
$6p_{1/2}$	$5f_{7/2}$	$4f_{7/2}$	$p_{1/2}$	0.0117	-0.132	-0.114	•		
$6p_{1/2}$	$5f_{5/2}$	$4f_{5/2}$	$p_{1/2}$	0.0145	0.136	0.146			
$5p_{3/2}$	$7f_{7/2}$	$4f_{7/2}$	$p_{3/2}$	0.0292	0.085	0.036			
$8s_{1/2}$	$5d_{5/2}$	$5s_{1/2}$	$d_{3/2}$	0.0090	0.065	0.064			
$5d_{3/2}$	$6f_{7/2}$	$4f_{7/2}$	$d_{3/2}$	0.0707	-0.033	0.056			
$5d_{3/2}$	$6f_{5/2}$	$4f_{5/2}$	$d_{3/2}$	0.0019	0.341	0.438			
$8s_{1/2}$	$5d_{5/2}$	$5s_{1/2}$	$d_{5/2}$	0.0134	0.065	0.064			
$5d_{5/2}$	$6f_{7/2}$	$4f_{7/2}$	$d_{5/2}$	0.0019	0.627	0.602			
$6p_{1/2}$	$6f_{5/2}$	$5p_{1/2}$	$f_{5/2}$	0.0540	-0.226	-0.004			
$8p_{1/2}$	$5d_{3/2}$	$5s_{1/2}$	$f_{5/2}$	0.0024	-0.204	-0.110			
$7f_{5/2}$	$5d_{5/2}$	$5s_{1/2}$	$f_{5/2}$	0.0015	-0.089	-0.096			
$8g_{7/2}$	$5d_{3/2}$	$5p_{1/2}$	$f_{5/2}$	0.0083	-0.087	0.133			
$8p_{3/2}$	$5d_{3/2}$	$5s_{1/2}$	$f_{7/2}$	0.0018	0.155	0.264			
$6f_{7/2}$	$6p_{1/2}$	$5p_{1/2}$	$f_{7/2}$	0.0758	-0.158	0.073			
$7f_{7/2}$	$5d_{5/2}$	$5s_{1/2}$	$f_{7/2}$	0.0033	-0.052	-0.060	$[1]\alpha$ and	β are	e the
$5g_{9/2}$	$6d_{3/2}$	$5p_{1/2}$	$f_{7/2}$	0.0011	-0.159	-0.119			
$6d_{3/2}$	$5g_{7/2}$	$5p_{1/2}$	$h_{9/2}$	0.0151	-0.196	-0.148			
$6d_{5/2}$	$5g_{7/2}$	$5p_{1/2}$	$h_{9/2}$	0.0028	0.040	0.129			
$5f_{5/2}$	$6p_{1/2}$	$4f_{5/2}$	$h_{9/2}$	0.0014	0.136	0.146			
$7f_{5/2}$	$5d_{5/2}$	$5s_{1/2}$	$h_{9/2}$	0.0094	-0.090	-0.096			
$7f_{5/2}$	$5p_{3/2}$	$4f_{7/2}$	$h_{9/2}$	0.0049	0.048	-0.003			
$5g_{7/2}$	$6p_{3/2}$	$5s_{1/2}$	$h_{9/2}$	0.0017	0.447	0.538			
$8g_{7/2}$	$5d_{3/2}$	$5p_{1/2}$	$h_{9/2}$	0.0566	-0.087	0.133			
$5d_{5/2}$	$7f_{5/2}$	$5s_{1/2}$	$h_{11/2}$	0.0012	-0.089	-0.096			
$6d_{5/2}$	$5g_{7/2}$	$5p_{1/2}$	$h_{11/2}$	0.0131	0.040	0.013			
$7f_{7/2}$	$5d_{5/2}$	$5s_{1/2}$	$h_{11/2}$	0.0193	-0.052	-0.060			
$7f_{7/2}$	$5p_{3/2}$	$4f_{7/2}$	$h_{11/2}$	0.0084	0.085	0.036			
$5g_{9/2}$	$6d_{3/2}$	$5p_{1/2}$	$h_{11/2}$	0.0242	-0.159	-0.118			
$5g_{9/2}$	$6p_{3/2}$	$5s_{1/2}$	$h_{11/2}$	0.0018	0.485	0.573			
$5g_{9/2}$	$6d_{5/2}$		$h_{11/2}$	0.0028	0.078	0.147			
$6g_{9/2}$	$5f_{5/2}$	$5p_{1/2}$	$i_{11/2}$	0.0053	0.084	0.157			
excited		n orbit		$d \gamma$ is the groun	d-state h	ole of the	e dielectror	nic doc	rway

excited electron orbitals, and γ is the ground-state hole of the dielectronic doorway state; εlj is the partial wave of the incident electron. [2]Direct term contributions to the dimensionless sum in Eq. (10), $\bar{\sigma}_c k^2/\pi^2$, using spreading width = 0.15 a.u. and configuration energy, with magnitudes greater than 5×10^{-3} . [3] $\Delta E = \varepsilon_{\alpha} + \varepsilon_{\beta} - \varepsilon_{\gamma}$ is the mean-field energy of the doorway state relative to the threshold. [4] ΔE is the configuration energy relative to the threshold.

present calculations show that excitations involving 4f orbitals are more important especially at threshold since they contribute significantly to the recombination cross sections. As expected, the energy dependences of the resonance and direct recombination rates are very close, although the latter is about 200 times smaller. There is a good overall agreement between the resonance rate and experimental data at electron energies between 1 eV and 100 eV. To compare with Au^{25+} , we calculated the rate coefficients for

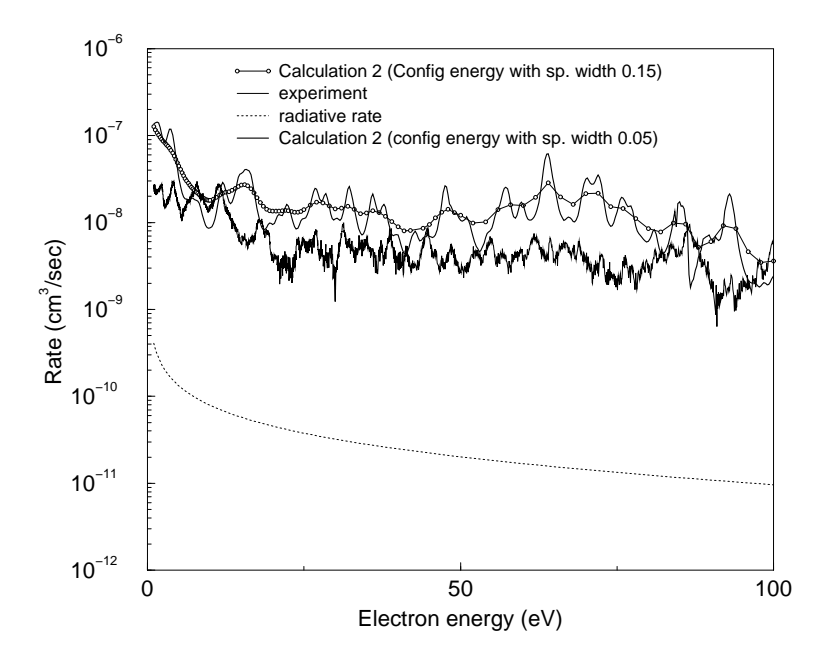


Figure 7. Electron recombination rate on U²⁸⁺. Open circles connected by solid line: Calculation 2 (using configuration energy and $\Gamma_{spread} = .15$ a.u.), Solid line: Calculation 2 (using configuration energy and $\Gamma_{spread} = 0.05$ a.u.), Dense solid line: Experiment, and Dotted line: Radiative rate.

the electron energy ranging from 1 eV to 100 eV. Because the previous calculation[20] was restricted to the energy range below 1 eV. Figure 9 shows results three different calculations and the experimental data. It may be seen that the present (we call our best calculation) calculation uses configuration energies shows a very good qualitative agreement with the experiment in comparison to the other two calculations. The RR is found be of smaller in magnitude. The most striking feature in this graph is that the experimental data quickly departs from the theoretical values as one goes to higher energies. This can be interpreted as that in this energy range the fluorescence yield certainly goes down from 1 which can be well understood from the Figure 10. In this figure we show the configuration energies as a function of total angular momentum J. It shows that due to the presence of a lots levels, many inelastic channels open up and they participate strongly. This situation makes the fluorescence yield less than 1 and hence the theory predicts recombination rates higher in magnitude.

Which in turn just opposite to the case of U^{28+} as shown in Figure 11.

Finally, we compare in table II, the present energies of the lowest configurations in U^{28+} with the energies calculated by using HULLAC code[17]. As mentioned

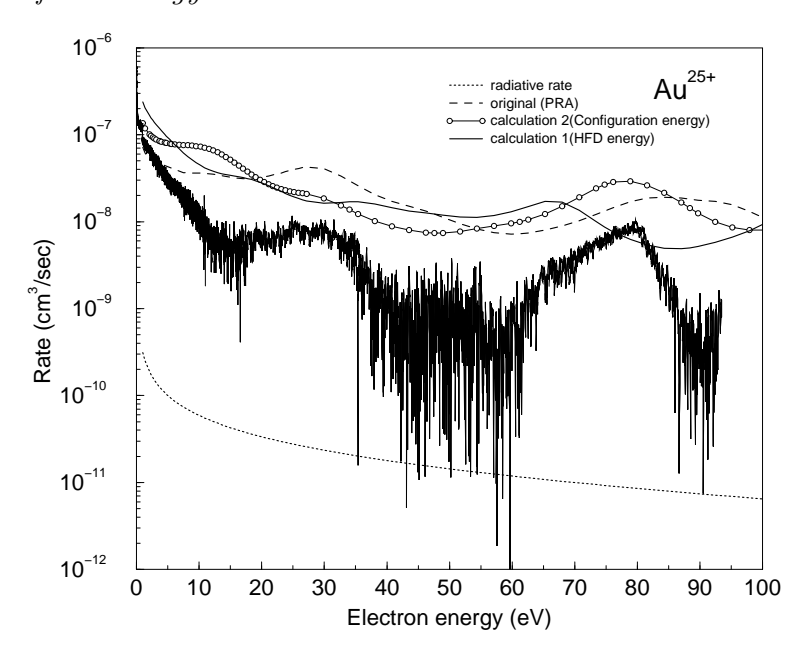


Figure 8. Electron recombination rate on $\mathrm{Au^{25+}}$. Open circles connected by solid line: Calculation 2 (using configuration energy and $\Gamma_{spread}=0.5$ a.u., Thick Solid line (using HFD energy and $\Gamma_{spread}=0.5$ a.u.), Thick dotted line: Original calculation (as in PRA 66, 012713 (2002)), Dense solid line: Experiment, and Dotted line: Radiative rate.

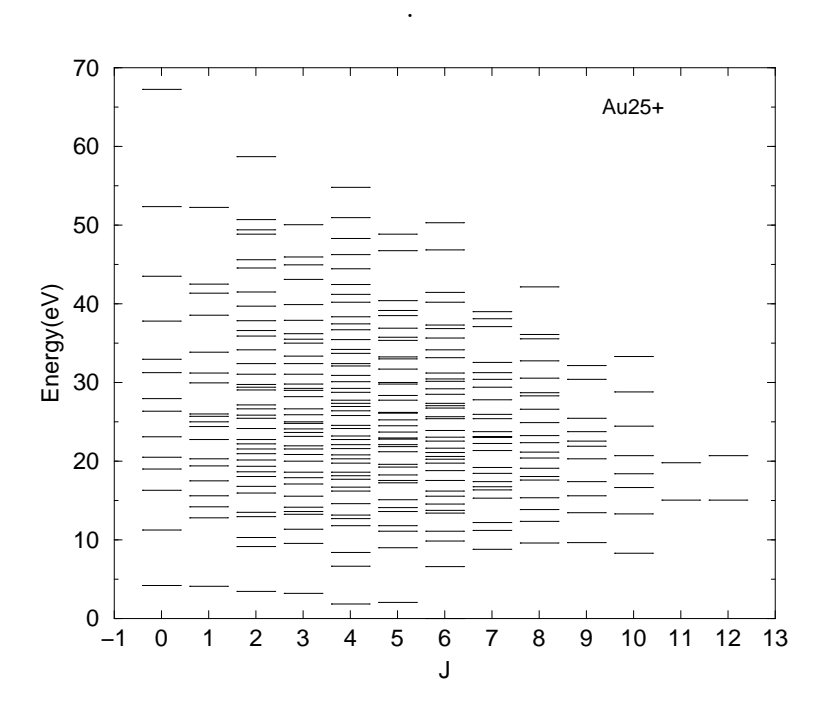


Figure 9. Spectrum of low lying excited states of Au^{25+} . All the levels shown belong to the $4f^8$ configurations. The ground state is characterized by J=6.

earlier that in Ref[17], energies have been calculated by using different codes such as multiconfiguration Hartree-Fock (MCHF), the AUTOSTRUCTURE code in the

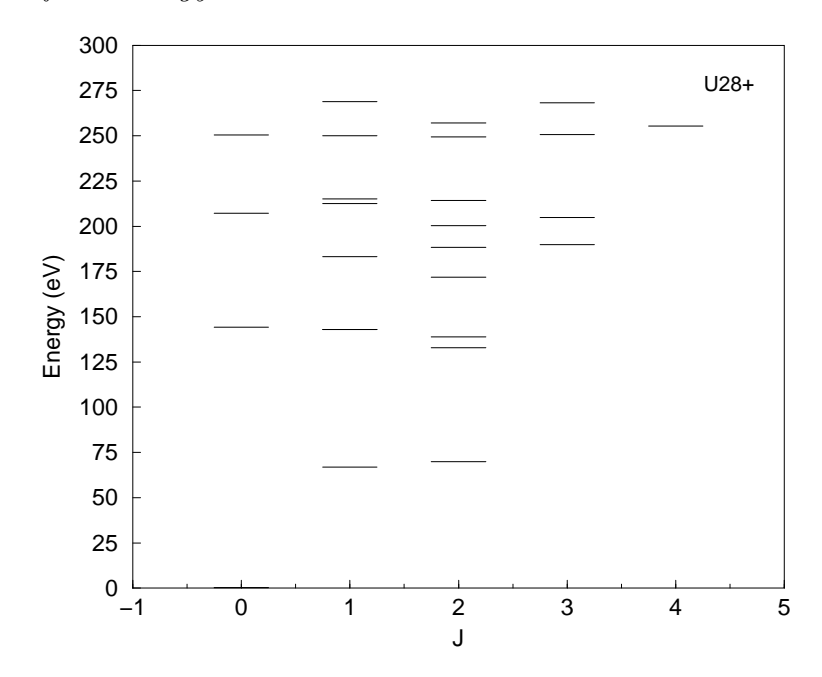


Figure 10. Spectrum of low lying excited states of U^{28+} . All the levels shown belong to $5s^25p^2$, $5s5p^3$ and $5s^25p5d$ configurations (see table II). Its ground state is characterized by J=0.

perturbative-relativistic [AS(PR)] and in the semirelativistic [AS(SR)] mode and the HULLAC code. On comparison we found the present energies are close to those obtained by Mitnik et. al. [17] using HULLAC code since both the calculations are fully relativistic.

5. Summary and outlook

We have shown that the dielectronic states weakly mix with each other and show a substantial mixing with complicated multiply excited states. This explains the mechanism of low energy recombination of electron with U^{28+} . The present results are found to be in good agreement with the experimental data. We found that one must not ignore the excitations from 4f orbitals while considering the low energy recombination of U^{28+} ion. On detailed study, we found the configuration mixing between the doubly excited states and multiply excited states is not complete or uniform. Although this theory is valid in a system having an extreme degree of configuration mixing [20], still it predicts quite good results for other systems where there is not enough strong configuration mixing, for example U^{28+} . This work develops further a statistical theory to study the low energy recombination process.

6. acknowledgements

We thank Prof. A. Müller for providing experimental data of Au^{25+} and U^{28+} in numerical form and for his stimulating discussions. We also thank to Dr. C. Harabati

Table 2. Energies of the lowest configurations in U^{28+} . The present calculated energies obtained by using Hartree Fock Dirac (HFD) code are compared with the energies calculated using HULLAC code [18]. The energies are in eV.

Carc	_		ie [16]. The energies
Configurations	Term(J)	HULLAC	HFD (present)
$5s^25p^2$	0	0.00	0.00
$5s^25p^2$	1	65.884	66.980
$5s^25p^2$	2	68.876	69.904
$5s5p^3$	2	131.80	132.94
$5s^25p^2$	2	137.24	138.80
$5s5p^3$	1	142.05	142.97
$5s^25p^2$	0	143.60	144.16
$5s^25p5d$	2	170.33	171.83
$5s^25p5d$	1	182.26	183.27
$5s^25p5d$	2	186.37	188.24
$5s^25p5d$	3	188.07	189.82
$5s5p^3$	2	198.49	200.24
$5s5p^3$	3	202.91	204.78
$5s5p^3$	0	205.43	207.29
$5s5p^3$	1	210.77	212.53
$5s5p^3$	2	212.50	214.21
$5s5p^3$	1	213.51	215.08
$5s^25p5d$	2	247.30	249.28
$5s5p^3$	1	287.25	250.11
$5s^25p5d$	3	248.65	250.66
$5s^25p5d$	0	248.40	250.40
$5s^25p5d$	4	252.64	255.34
$5s^25p5d$	2	254.29	257.00
$5s^25p5d$	3	266.20	268.30
$5s^25p5d$	1	266.67	268.86

for allowing us to make use of his codes as well as for his useful comments. Financial help from EPSRC is highly acknowledged.

7. References

- [1] M. Arnaud and R. Rsthenflug, APJ, 398, 394(1985).
- [2] M. Holzscheiter and M. Charlton, Rep. Prog. 62,1 (1999).
- [3] H. S. W. Massey and D. R. Bates, Rep. Prog. Phys. 9, 62 (1943).
- [4] Recombination of Atomic Ions, NATO ASI series, Series B: Physics: vol. 296, Eds. W. G. Graham, W. Fritsch, Y. Hahn, and J. A. Tanis (Plenum Press, New York, 1992).
- [5] L. H. Andersen, P. Hvelplund, H. Knudsen, and P. Kvistgaard, Phys. Rev. Lett. 62, 2656 (1989).
- [6] G. Kilgus et al., Phys. Rev. Lett. 64, 737 (1990).
- [7] S. Schennach et al., Z. Phys. D 30, 291 (1994).

- [8] H. Gao et al., Phys. Rev. Lett. **75**, 4381 (1995).
- [9] R. Shuch et al., Hyperfine Interact. 99, 317 (1996).
- [10] O. Uwira et al., Hyperfine Interact. 99, 295 (1996).
- [11] O. Uwira et al., Hyperfine Interact. 108, 149 (1997).
- [12] W. Zong et al., Phys. Rev. A 56, 386 (1997).
- [13] S. Mannervik et al., Phys. Rev. Lett. 81, 313 (1998).
- [14] D. R. DeWitt et al., Phys. Rev. A 50, 1257 (1994); D. R. DeWitt et al., J. Phys. B 28, L147 (1995).
- [15] D. R. DeWitt et al., Phys. Rev. A 53, 2327 (1996).
- [16] A. Hoffknecht et al., J. Phys. B 31, 2415 (1998).
- [17] D. M. Mitnik et al., Phys. Rev. A 57, 4365 (1998).
- [18] G. F. Gribakin, A. A. Gribakina, and V. V. Flambaum, Aust. J. Phys. 52, 443 (1999); see also physics/9811010.
- [19] G. F. Gribakin and S. Sahoo, J. Phys. B: At. Mol. Opt. Phys. 36 3349 (2003).
- [20] V. V. Flambaum, A. A. Gribakina, G. F. Gribakin and C. Harabati, Phy. Rev. A 66, 012713 (2002).
- [21] A. Bohr and B. Mottelson, Nuclear structure, Vol. 1 (Benjamin, New York, 1969).
- [22] J. N. Ginocchio, Phys. Rev. Lett. 31, 1260 (1973); J. Bauche and C. Bauche-Arnoult, J. Phys. B 20, 1659 (1987).
- [23] This fit is valid for E > 1 a.u. In the Fermi-gas model a is related to the single-particle level density at the Fermi level $g(\varepsilon_F) = 3a^2/2\pi^2$. The fitted value a = 3.99 gives $g(\varepsilon_F) = 2.4$ a.u., in agreement with the orbital spectrum in Fig.1
- [24] L. D. Landau and E. M. Lifshitz, Quantum Mechanics, 3rd ed. (Pergamon, Oxford, 1977).
- [25] Here we assume that the electron energy is below the target excitation threshold.
- [26] V. Zelevinsky, B. A. Brown, M. Frazier, and M. Horoi, Phys. Rep. 276, 85 (1996).
- [27] V. V. Flambaum, A. A. Gribakina, G. F. Gribakin, and M. G. Kozlov, Phys. Rev. A 50, 267 (1994); V. V. Flambaum, A. A. Gribakina, and G. F. Gribakin, Phys. Rev. A 54, 2066 (1996); 58, 230 (1998).
- [28] V. V. Flambaum and O. K. Vorov, Phys. Rev. Lett. 70, 4051 (1993).
- [29] D. C. Griffin, M. S. Pindzola, and C. Bottcher, Phys. Rev. A 31, 568 (1985).